nature machine intelligence

Article

https://doi.org/10.1038/s42256-026-01245-5

Learning the coupled dynamics of global climate modes

Received: 12 October 2025

Accepted: 20 April 2026

Published online: 01 June 2026

Check for updates

Yuan Yuan[1,2], Jingtao Ding[1,2], Zhongpu Qiu[3], Jingfang Fan[3,4] ✉ & Yong Li[1,2] ✉

Global weather extremes, from monsoons to droughts, are shaped by a network of recurrent, coupled ocean–atmosphere patterns known as climate modes. These modes, spanning from the Pacific's El Niño-Southern Oscillation to interconnected patterns in the Indian and Atlantic Oceans, form a dynamically linked global system governed by complex nonlinear interactions. Holistically forecasting this interconnected system—rather than treating modes in isolation or in simplified pairs as existing approaches do—remains a fundamental challenge in machine intelligence for complex systems. Here we introduce UniCM, a unified deep model for global climate modes forecasting. Its key innovation lies in a dual-branch architecture that learns the dynamics of a coupled system directly from data, achieving a truly unified prediction through the synergistic modelling of localized dynamics and their collective global couplings. UniCM achieves strong performance in unified global climate-mode forecasting, outperforming strong existing baselines and extending the skilful forecast lead time across multiple major climate modes. It successfully captured the diversity of historical events, from the extreme 1997–1998 El Niño to the prolonged and challenging 2020–2023 triple-dip La Niña. Beyond accuracy, UniCM offers interpretability; its internal attention mechanism identifies dynamic precursors and quantifies the structured inter-mode interactions that precede extreme climate events. Our results demonstrate that learning the coupled dynamics of climate modes as an interconnected system unlocks emergent predictability, laying a foundation for unified forecasting and data-driven insights that deepen our understanding of global ocean–atmosphere dynamics.

Large-scale climate variability on seasonal-to-interannual timescales shapes weather extremes, ecosystem dynamics and the stability of critical sectors such as agriculture, water resources and disaster preparedness[1,2]. Much of this variability is driven by a network of recurring, coupled ocean–atmosphere patterns known as climate modes[3–6]. While the El Niño-Southern Oscillation (ENSO) in the Pacific[7–10] and the Indian Ocean Dipole (IOD)[11,12] are the most recognized of these phenomena, they are components of a larger, interconnected system[13]. Other modes, including the North and South Pacific Meridional Modes (NPMM and SPMM), Indian Ocean Basin (IOB), Southern Indian Ocean Dipole (SIOD) and Tropical North Atlantic (TNA) variability, also exert substantial regional and global influence[13–18]. Crucially, these modes do not evolve in isolation. They form a dynamically linked global system[15], exchanging energy across ocean basins through intricate teleconnections[19] that ultimately control the timing and intensity of monsoons, droughts and floods worldwide[1,11,12,19].

[1]Department of Electronic Engineering, Tsinghua University, Beijing, China. [2]Beijing National Research Center for Information Science and Technology, Tsinghua University, Beijing, China. [3]School of Systems Science, Beijing Normal University, Beijing, China. [4]Potsdam Institute for Climate Impact Research (PIK), Potsdam, Germany. ✉e-mail: Jingfang@bnu.edu.cn; liyong07@tsinghua.edu.cn

The interconnected nature of these climate modes underscores the profound difficulty of modelling them as a unified, coupled system[3]. These modes span vast spatiotemporal scales and interact through nonlinear, state-dependent couplings that vary seasonally and with background climate conditions[8,15,20–22]. Consequently, existing approaches that treat modes in isolation or via simple pairwise correlations are fundamentally inadequate to capture the emergent, collective behaviours of the global system[10,23,24]. This challenge is compounded by limited physical understanding of many non-ENSO modes[14], constraining even the state-of-the-art extended nonlinear recharge oscillator (XRO)[13], which relies on an ENSO-centric design with linear assumptions. While recent work has explored physics-guided deep echo state networks (DESN) to extend ENSO predictability[25], the broader challenge of learning the coupled dynamics of multiple climate modes as an interconnected, cross-scale system remains largely unresolved. Addressing this gap requires models that can learn the complex structure of these couplings directly from data, providing a foundation for unified seasonal-to-interannual forecasting of global climate modes.

A key insight for overcoming these challenges is that climate modes are not abstract entities acting independently. Their complex, state-dependent interactions are governed by their connection to the underlying physical system from which they emerge. From a bottom-up perspective, climate modes are large-scale emergent structures arising from the fine-grained dynamics of physical fields, such as sea surface temperature (SST)[13]. From a top-down perspective, once formed, these modes are no longer passive indicators. They act as organizing forces that interact and collectively steer the future evolution of both the physical fields that generate them and the broader climate system[6,13]. Successfully modelling this feedback loop—where fields generate modes, and modes, in turn, regulate those fields—is the key to unlocking their joint predictability.

Here we introduce UniCM, a unified deep learning framework for global climate modes forecasting, designed with structured inductive biases that enable hierarchical, coupling-aware representation learning. Unlike conventional approaches that treat climate modes as isolated problems, UniCM models them as an interconnected global system by capturing coupled dynamics at two critical levels: (1) the local-to-global emergence between fine-grained physical fields and large-scale climate patterns and (2) the nonlinear feedback among the climate modes themselves. This approach operates on the principle that the predictability of the climate system is an emergent property of these multi-scale couplings. To realize this, the architecture uses a dual-view Transformer that explicitly synchronizes bottom-up physical dynamics with top-down systemic regulation. Specifically, the Globalformer branch first models the spatiotemporal evolution of fine-grained physical fields, such as SST and surface wind stress, capturing the bottom-up processes from which large-scale climate modes emerge. On top of this physical representation, the Modeformer branch abstracts the collective temporal dynamics and nonlinear interactions among climate modes, forming a compact, system-level representation of the coupled climate state. These learned mode representations are then injected back into the physical field space through a cross-view coupling mechanism, enabling a top-down, coupling-aware guidance that regulates the Globalformer's learning and prediction.

UniCM outperforms XRO in multi-mode prediction and surpasses DESN in long-range ENSO forecasting. It extends to 19 months for ENSO forecasting and to 7 months for IOD, while also substantially improving the prediction skill for other less-studied modes by more than 22% on average. Moreover, it captures the diversity of historical events, from the extreme 1997–1998 El Niño to the challenging 2020–2023 triple-dip La Niña[26–28]. Beyond prediction, UniCM reveals physically meaningful early-warning signals. We found that localized precursor patterns and highly structured cross-mode interactions consistently emerged preceding extreme climate events. For instance, the model independently identified the NPMM as a key precursor to the 1997 El Niño, a finding consistent with recent physics-based studies[29], that highlighted the NPMM's sustained influence on El Niño evolution. UniCM's ability to uncover such relations without previous physical assumptions demonstrates that a unified, coupling-aware approach not only enhances predictability but also advances the fundamental understanding of the interconnected climate system. The architectural principles of UniCM hold the potential to be extended to other complex systems where components and global structures exhibit similar co-evolutionary patterns[30–32].

A unified model for forecasting global climate modes

Multi-view architecture for learning multi-scale coupled dynamics

At its core, UniCM uses a multi-view Transformer architecture that analyses the climate system from two distinct yet complementary perspectives (Fig. 1a). The Globalformer branch models the spatiotemporal evolution of fine-grained physical climate fields. It processes five key variables—SST (T), zonal and meridional surface wind stress (τ_x, τ_y), thermocline depth (h_T) and upper-ocean temperature across 300-m depth (T_{300})—to capture the bottom-up processes that give rise to climate modes. These variables are anomaly-normalized, interpolated onto a 5° × 5° grid covering 0° E–360° E and 40° S–0° N, and subsequently tokenized into spatial patches for Transformer encoding. This 5° × 5° resolution is selected to align with the characteristic spatial scales of target climate modes while acting as a physical low-pass filter to suppress unpredictable synoptic noise[33,34]. In parallel, the Modeformer branch models the collective temporal evolution of seven key climate-mode indices: ENSO, IOD, TNA, NPMM, SPMM, IOB and SIOD. These indices, computed from SST fields following established definitions[13], are smoothed with a 3-month running mean and structured as input sequences. The Modeformer is designed to autoregressively forecast the mode trajectory while simultaneously constructing a mode representation to explicitly capture their dynamic interactions. Both branches are built on a spatiotemporal Transformer backbone with separate attention mechanisms for the spatial and temporal dimensions, ensuring computational scalability for high-dimensional climate data (Fig. 1b).

Coupling-aware mechanism

A central innovation of UniCM lies in its coupling-aware learning of climate interactions and dynamics. The first level of coupling is learned within the Modeformer, which explicitly models the complex, nonlinear interactions and temporal co-evolution among the climate modes. Using a mode-wise attention mechanism, it captures dynamic interdependencies and teleconnections between patterns such as ENSO, IOD and TNA, yielding a high-level representation of the entire climate-mode system's current state and trajectory. The second level of coupling is realized through the cross-view mechanism, which connects this high-level system state back to the underlying physical reality. The synthesized representation of inter-mode dynamics learned by the Modeformer is not kept isolated; instead, it is injected as a guiding bias into the Globalformer. This 'mode-to-patch guidance' ensures that the model's fine-grained forecasts of physical fields (for example, SST) are dynamically informed by and consistent with the state of the large-scale climate patterns. By learning couplings at both the inter-mode and the mode-field levels, UniCM captures the critical feedback loop that governs the global climate system.

Results

Improved prediction skill for ENSO

We first evaluated UniCM's performance using the anomaly correlation coefficient (ACC), a core metric that verifies a model's skill in predicting the pattern of climate anomalies[13,34,35]. To rigorously test the model's

https://doi.org/10.1038/s42256-026-01245-5

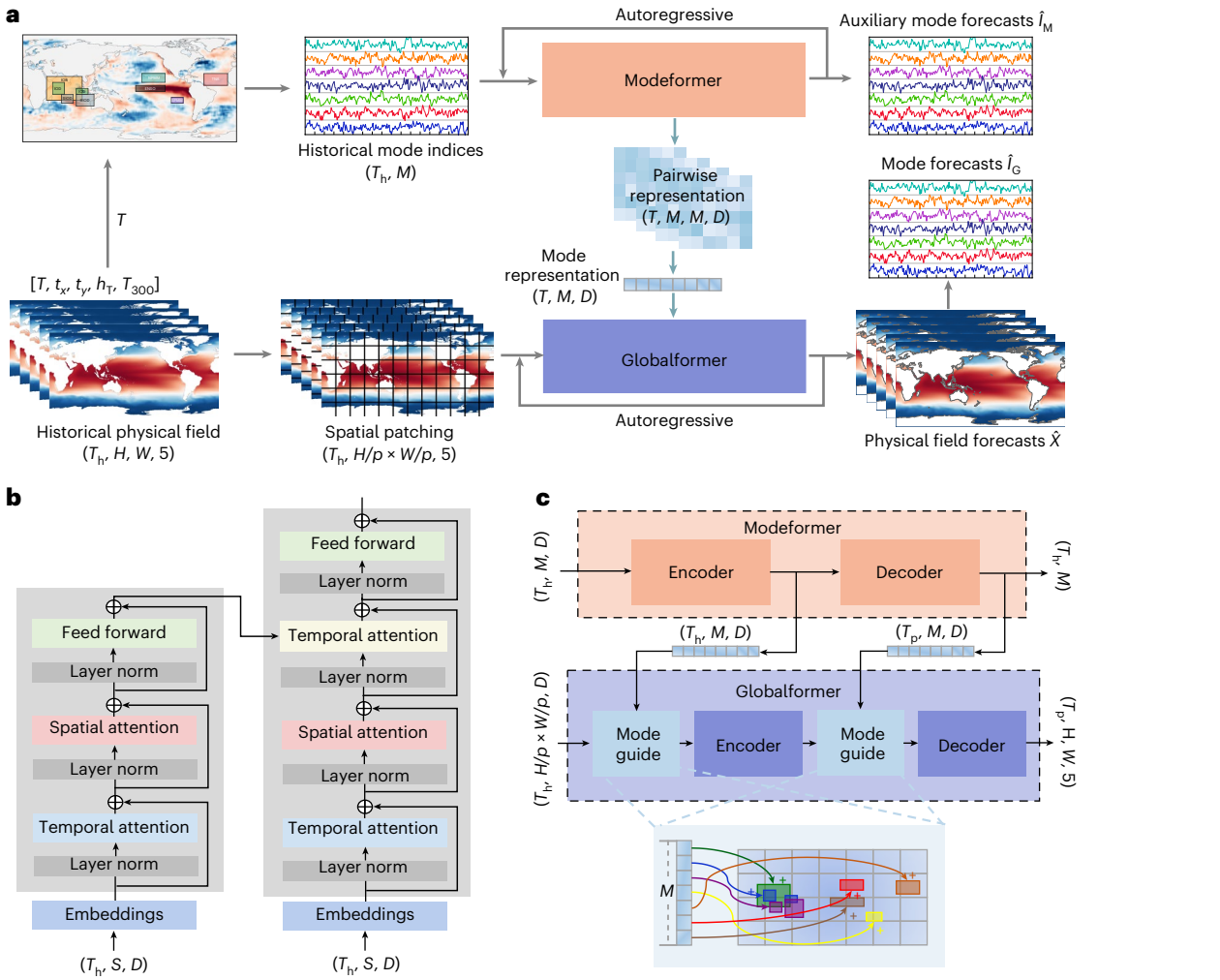

Fig. 1 | Overview of the UniCM architecture. a, The model processes two complementary input streams. The bottom stream consists of historical physical fields comprising five ocean–atmosphere variables: SST (T), zonal surface wind stress (τ_x), meridional surface wind stress (τ_y), thermocline depth (h_T) and upper-ocean temperature averaged over the top 300 m (T_{300}). These fields are interpolated onto a 5° × 5° grid and divided into non-overlapping spatial patches, forming a tensor of shape (T_h, $H/p \times W/p$, 5), where T_h denotes the number of historical input time steps (indicated by the upward arrow labelled T in the figure), $H/p \times W/p$ is the number of spatial patches and 5 refers to the five physical variable channels. The top stream encodes seven climate-mode indices as a multivariate time series of shape (T_h, M), where M is the number of modes. Two Transformer branches, the Globalformer and the Modeformer, process the physical fields and climate-mode sequences, respectively, interacting via a learned pairwise mode representation. **b**, The backbone of the Transformer layers, featuring temporal and spatial attention mechanisms. The left panel shows the encoder block and the right panel shows the decoder block. Layer norm, layer normalization. **c**, The encoder–decoder architecture of both branches. The Globalformer incorporates mode guidance by injecting representations from the Modeformer into corresponding spatial locations.

real-world applicability and generalization, UniCM was directly evaluated on four reanalysis datasets: the Global Ocean Data Assimilation System (GODAS), ECMWF Reanalysis v.5 (ERA5), Ocean Reanalysis System v.5 (ORAS5) and Simple Ocean Data Assimilation v.2.2.4 (SODA). We note that ORAS5 and ERA5 share the same prescribed SST boundary conditions and thus do not constitute fully independent validations for SST-derived indices. As shown in Fig. 2a, UniCM achieved consistently much higher prediction skill than baseline models (ResoNet[35], XRO[13], CNN[34] and recent DESN[25]) across the entire 24-month forecast horizon. Notably, UniCM extended the skilful forecast lead time, maintaining an ACC above the critical 0.5 threshold for 19 months. This extends the predictability limit to 19 months, surpassing DESN at 16 months and standard deep learning baselines, including CNNs and Transformers, at 15 months, under our out-of-distribution evaluation protocol (Supplementary Section 1.1). This suggests that the gain arises from learning cross-scale couplings, including both inter-mode interactions and the feedback between large-scale climate modes and fine-grained physical fields. This advantage in correlation was corroborated by error-based metrics; UniCM reduced the root mean square error (r.m.s.e.) by more than 14.1–17.9% relative to baselines, indicating a more accurate prediction of event magnitudes (Supplementary Figs. 3,5,7 and 8). Furthermore, the model's performance proved robust, maintaining strong ACC scores of 0.78–0.8 for 12-month lead times across multiple observational datasets such as ERA5, GODAS and SODA v.2.2.4 (Supplementary Figs. 2,4 and 6).

A formidable challenge for ENSO prediction is the 'spring predictability barrier', a period in the boreal spring when forecast skill tends to decline sharply[36]. UniCM has demonstrated the ability to overcome this barrier. For forecasts targeting the spring seasons (March, April and May and April, May and June, highlighted in yellow), UniCM sustained an ACC greater than 0.5 for lead times up to 14 months (Fig. 2b). This stands in contrast to baseline models, which lose skilful predictive power (ACC < 0.5) at forecast horizons ranging from 9 months to 12 months (Supplementary Figs. 9–12). This sustained performance

https://doi.org/10.1038/s42256-026-01245-5

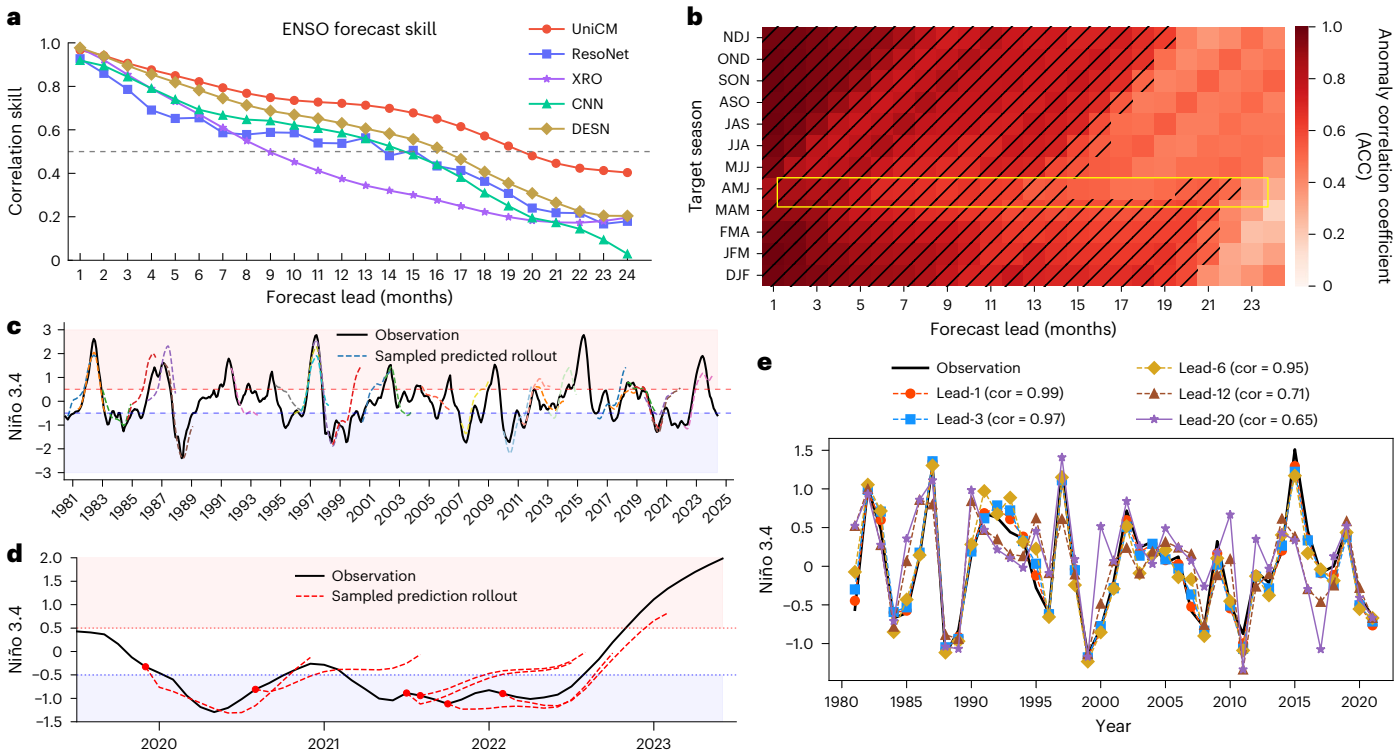

Fig. 2 | ENSO forecast performance of UniCM. a, ACC for the Niño 3.4 index as a function of forecast lead time. UniCM (red) is compared against baseline models: XRO (purple), ResoNet (blue), CNN (green) and DESN (light brown). Forecasts are verified against observations from 1980 to 2023. **b**, Heatmap of ACC scores showing seasonal forecast skill. The skill is plotted against target season (*y* axis) and forecast lead (*x* axis). The yellow box highlights the boreal spring season (March, April, May (MAM), April, May June (AMJ)), a period known for the spring predictability barrier. **c**, Time series of the observed Niño 3.4 index (solid black line) from 1980 to 2023, overlaid with hindcast predictions from UniCM (dashed lines) initiated from various start months. **d**, A magnified view of **c** focusing on the 2020–2023 triple-dip La Niña event. Observed values (black) are compared with UniCM's predictions (red dashed lines). **e**, Comparison of the observed Niño 3.4 index (black line) with forecasts made at discrete lead times: 1 month, 3 months, 6 months, 12 months and 20 months. The legend reports the ACC score associated with different lead times. cor, correlation.

through the spring predictability barrier highlights a key advantage of UniCM for reliable, year-round operational forecasting. Figure 2e provides a granular look at performance across different forecast horizons. The predictions show remarkable fidelity at short leads (1–6 months, ACC > 0.95) and, critically, remain highly skilful at extended horizons of 12 months and even 20 months. At these longer leads, the model consistently captures the correct phase and relative magnitude of major ENSO events, maintaining robust ACC scores of 0.71 and 0.65, respectively. This visual evidence confirms that UniCM's long-range skill is not an anomaly, but reflects a genuine capacity to forecast core ENSO dynamics.

UniCM's skill extended beyond statistical averages to accurately capture the diverse characteristics of individual ENSO events. The hindcast of the Niño 3.4 index from 1980 to 2023 illustrates the model's ability to reproduce the amplitude, timing and duration of historically notable events (Fig. 2c). This success is particularly meaningful because different event types are known to arise from distinct physical mechanisms. For instance, some events, such as the canonical 1982–1983 and 1997–1998 El Niños also captured by the model, are driven by strong thermocline feedbacks in the Eastern Pacific[37]. In contrast, others, such as the Central Pacific or 'Modoki' events (the 1991–1992 El Niño), are associated with warming further west[38,39]. UniCM's ability to predict this wide spectrum of event types suggests it has learned the key spatiotemporal dependencies governing ENSO dynamics, rather than overfitting to a single event category. The model's robustness was further validated against the recent 2020–2023 triple-dip La Niña[26–28] (Fig. 2d), where it correctly predicted the onset, intensity and decay of three consecutive La Niña phases. This rare, multi-year event posed a formidable challenge to forecasting systems, as many conventional models struggle with La Niña's persistence and are prone to incorrectly forecasting a return to El Niño conditions[14,40].

System-level predictability of global climate modes

To demonstrate UniCM's capability to forecast global climate modes within a single, unified framework, we evaluated its performance on seven key modes spanning the Pacific, Indian and Atlantic Oceans, including IOD, IOB, SIOD, SPMM, NPMM and TNA. While ENSO remains the most predictable, many of these modes are characterized by greater stochasticity and complex regional drivers, posing a substantial challenge to forecasting[13,15–18]. To demonstrate the advantage of neural network-based coupling-aware modelling, We compared UniCM against representative baselines from different methodological families, including the fixed-operator regression model XRO[13] and the physics-guided nonlinear DESN[25], which provides a strong recent benchmark for ENSO forecasting. As shown in Fig. 3a, UniCM consistently achieved the strongest overall performance across the tested modes. In particular, while DESN provides a strong benchmark for ENSO prediction, UniCM further extends this advantage to a unified multi-mode setting by explicitly learning both inter-mode couplings and their interactions with the underlying physical fields. This superiority was most pronounced for modes governed by complex, state-dependent teleconnections. For instance, the forecast skill of XRO for TNA, SIOD and IOB, which relies on linear assumptions, collapsed below the 0.5 correlation threshold within 5–6 months (Supplementary Figs. 17–22). In contrast, UniCM maintained skilful predictions (ACC ≈ 0.5) for these same modes at lead times approaching 24 months (Fig. 3d and Supplementary Figs. 17–22). We further performed field-significance testing to verify the robustness of these results (Supplementary Figs. 23

https://doi.org/10.1038/s42256-026-01245-5

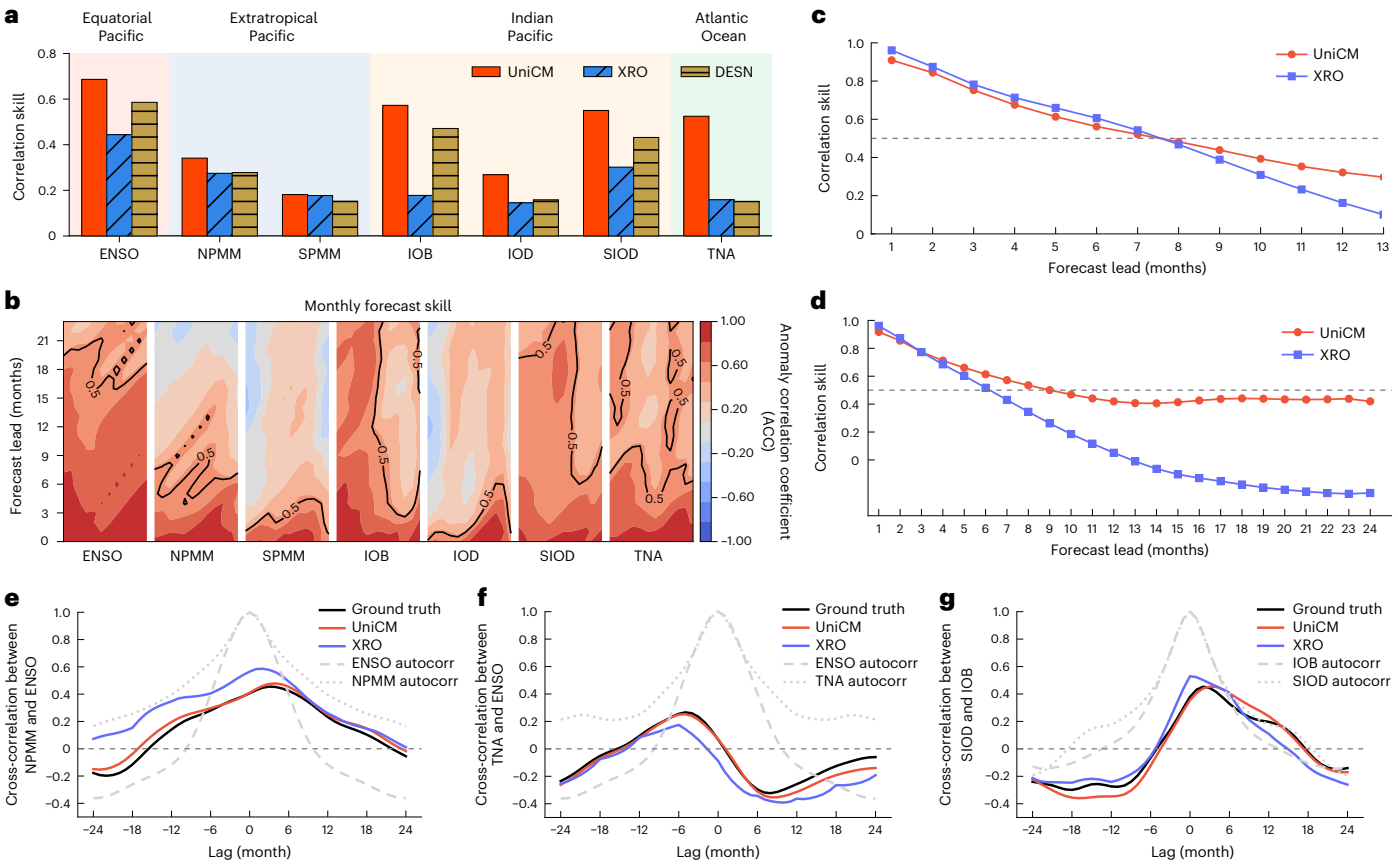

Fig. 3 | UniCM's performance on forecasting global climate modes. a, Average 24-month forecast skill (ACC) for UniCM, XRO and DESN across seven climate modes in the Equatorial Pacific, Extratropical Pacific, Indian Ocean and Atlantic Ocean. **b**, Heatmap of monthly forecast skill (ACC) for each climate mode as a function of lead time. Contour lines indicate correlation levels at 0.5 intervals. **c**,**d**, Forecast skill (ACC) over lead time for the NPMM (**c**) and TNA (**d**) modes, comparing UniCM (red) with XRO (blue). **e**–**g**, Lagged cross-correlations among key climate indices, including NPMM–ENSO. Autocorr denotes the lagged autocorrelation of each mode index, reflecting its temporal persistence. (**e**), TNA–ENSO (**f**) and SIOD–IOB (**g**) indices. Lines represent observations (black), UniCM forecasts (red) and XRO forecasts (blue). Additional lagged cross-correlations are available in Supplementary Section 4.

and 24). Notably, this system-level predictability is achieved with high data efficiency. Supplementary Fig. 39b shows that UniCM attains over 90% of its full-data performance using only 40% of the training samples, while temporally contiguous subsets lead to noticeably degraded skill. This suggests that exposure to diverse climatological states, rather than dense temporal sampling, is essential for learning climate-mode dynamics. Further ablation studies on model architecture design and hyperparameter sensitivity are provided in Supplementary Section 5.

To understand the capability of global prediction, we analysed the seasonal forecast skill for each mode (Fig. 3b). The results reveal distinct predictability windows: the IOD peaks in boreal autumn (September, October and November), the IOB in early spring (February and March) and the TNA in late summer (July, August and September), among others. These findings are consistent with previous observational and modelling studies[11,17,21,41–43]. However, UniCM extends these findings by providing a systematic, comparative assessment of seasonal predictability across this diverse set of modes within a single framework. This unified approach marks an improvement over the baseline models, which struggle to maintain skill across different seasons for many modes (Supplementary Fig. 13). This holistic view reveals that the temporal alignment of these predictability windows is not a coincidence, but is instead shaped by the dynamics of their interactions. For instance, the overlapping peak seasons of ENSO, IOD and TNA during the boreal autumn (September to November) suggest a period of heightened inter-modal influence. The model's internal attention mechanism (discussed with Fig. 5) validates this perspective, demonstrating that a joint modelling approach is necessary to uncover these critical, system-level couplings.

The physical realism of these learned couplings was further confirmed by UniCM's ability to reconstruct the observed lagged correlations between ENSO and other modes (Fig. 3e–g). The model precisely captures the timing, magnitude and asymmetry of these teleconnections, substantially outperforming XRO. For instance, UniCM accurately reproduces the ~4-month lead of NPMM on ENSO with a peak correlation of $r \approx 0.45$ (Fig. 3e), the bimodal TNA–ENSO correlation structure including the negative trough at a 7-month lag and the preceding positive peak (Fig. 3f), and the SIOD–IOB peak correlation ($r \approx +0.4$) at a 3-month lag (Fig. 3g). In contrast, the linear XRO model consistently overestimates coupling strengths, misplaces peak lead times and fails to capture asymmetric correlation structures. This advantage is even more pronounced in non-ENSO correlations, including intra-Pacific (SPMM–NPMM) and inter-basin (IOB–NPMM, TNA–IOB) interactions, where XRO's simpler, ENSO-centric assumptions prove inadequate (Supplementary Figs. 31–34). All reported peak correlations were statistically significant ($P < 0.001$). By accurately reproducing the observed lagged correlations between modes, UniCM provides a data-driven framework to learn and understand the coupled dynamics that govern the global climate system.

Skilful SST forecasting

To validate that UniCM's high skill on abstract mode indices is grounded in physically realistic forecasts, we evaluated its performance on the

https://doi.org/10.1038/s42256-026-01245-5

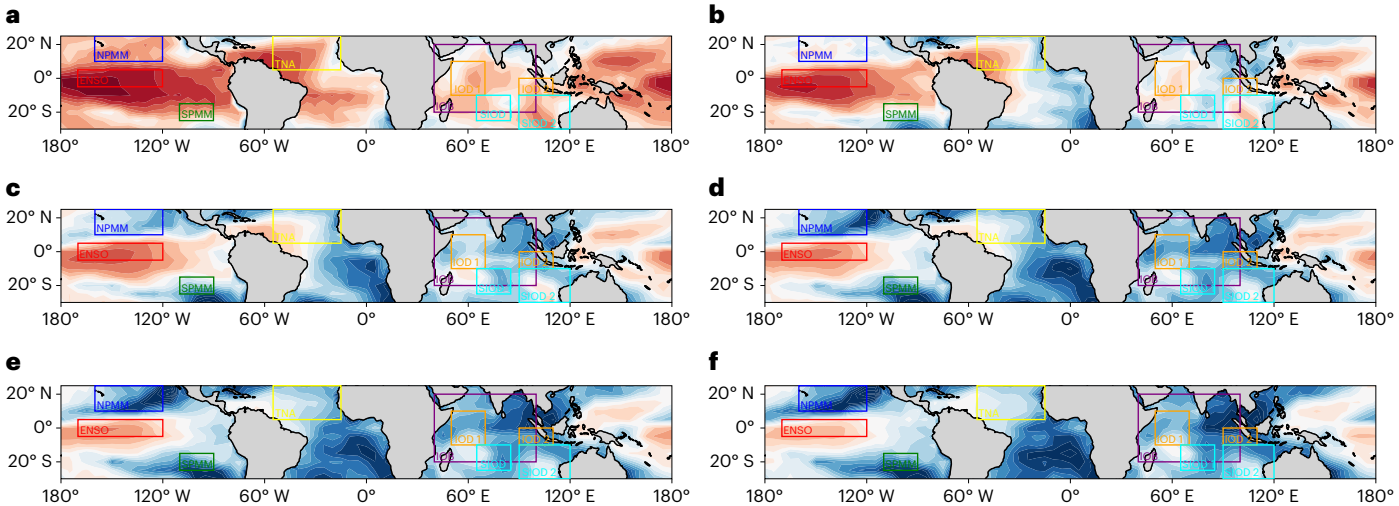

Fig. 4 | Spatial prediction skill of SST across different lead times. a–f, Spatial maps of the ACC for SST forecasts at lead times of 1 month (**a**), 3 months (**b**), 6 months (**c**), 9 months (**d**), 12 months (**e**) and 15 months (**f**). Boxes delineate regions corresponding to major climate modes. The model shows high fidelity in the Equatorial Pacific, a critical region for ENSO, and displays a physically realistic decay in skill with increasing lead time. Predictive signals are retained in key regions even at extended horizons of 12–15 months.

SST fields at a 5° × 5° resolution (Fig. 4). For subseasonal forecasts (1–3 months lead), UniCM demonstrates high skill (Fig. 4a,b), particularly over the Central and Eastern Equatorial Pacific, where it accurately captured core ENSO-related SST anomalies with an ACC greater than 0.8. As the forecast horizon extended to 6 months (Fig. 4c), the skill decayed progressively, which is a realistic pattern of diminishing predictability, yet it remained robust (ACC >0.6) in the Central Pacific basin, indicating the model's capacity to generalize from subseasonal signals to seasonal timescales. These results demonstrate a realistic decay of forecast skill consistent with known climate dynamics. Furthermore, the model's physical realism was tested against a well-documented forecasting challenge: the spring predictability barrier. We evaluated its ability to maintain skill at long-lead times that extend through this period. Around a 9-month lead (Fig. 4d), while its skill predictably declined in alignment with this barrier, it retained localized skill in key precursor regions such as the eastern Equatorial Pacific. Most notably, at an extended lead time of 12 months and even 15 months (Fig. 4e,f), the model maintained faint but coherent signals in the Niño 3.4 region. The persistence at long leads provides evidence that UniCM has learned the long-term evolution of core climate dynamics, rather than simply extrapolating initial conditions. This ability to produce physically plausible SST forecasts provides evidence that the model's predictive skill for climate modes is not a statistical artefact but is rooted in a representation of climate processes with physical meaning.

We further benchmarked UniCM against recent Transformer-based S2S models, FuXi-S2S[44] and CAS-Canglong[45], which target high-resolution field-wise forecasting. At a 12-month lead time, UniCM achieves a global mean ACC of 0.379, substantially higher than those of FuXi-S2S (0.262) and CAS-Canglong (0.207) (Supplementary Fig. 29). This advantage is most pronounced in the Equatorial Pacific, where UniCM preserves coherent large-scale SST anomaly patterns, whereas field-centric S2S models show rapidly degraded signals. As the Equatorial Pacific acts as the pacemaker of the global coupled climate system[7,15,46], UniCM's superior skill in this region underscores its advantage as a physically consistent foundation for long-lead climate forecasting.

Precursors and couplings revealed by UniCM

To probe the mechanisms underlying UniCM's predictive success, we analysed its internal attention mechanism, which provides an interpretable map of its decision-making process. Specifically, we used a two-pronged analysis to probe what the model has learned as predictive signals for major ENSO events: (1) we analysed the spatial attention distributions over physical fields to pinpoint key geographic regions, and (2) we examined the cross-mode attention matrices to quantify the dynamic interactions among climate modes that precede these events.

Figure 5a–f presents the spatial attention maps for six representative ENSO years (1983 El Niño, 1995 La Niña, 1996 La Niña, 1997 El Niño, 1999 La Niña, 2010 La Niña), while Fig. 5g,h illustrates two normal years (1980 and 1991). For the strong El Niño events of 1983 and 1997 (Fig. 5a,d), UniCM concentrated 65.3% and 76.9% of the strongest attention weights (top decile) in the Central and Eastern Equatorial Pacific, regions known to be critical for thermocline feedbacks that drive ENSO development. In contrast, during normal years such as 1980 and 1991 (Fig. 5g–h), attention patterns are diffuse, indicating a weakly coupled and unstructured state of the climate system. This contrast demonstrates the model's ability to distinguish between predictively relevant precursor patterns and background climate noise. Crucially, UniCM captures the known diversity of ENSO precursors. In the 1995 La Niña, attention shifted away from the Pacific to the tropical Atlantic, with 53.8% of the top-decile weights concentrated in that basin (Fig. 5b). This finding is consistent with established literature on inter-basin teleconnections where Atlantic SST anomalies can trigger Pacific cooling[20,41]. By contrast, the 1996 and 2010 La Niña events show stronger attention over the western Pacific, with 69.2% of the top-decile attention weights concentrated in that region, indicating the role of cold SST anomalies and reversed wind patterns in that region[47]. These case studies show that UniCM did not rely on a fixed precursor template but learned multiple physical pathways.

Beyond identifying spatial precursors, UniCM learns quantitative interaction principles that function as an early-warning system by identifying the transition from stochastic noise to organized, non-random coupling. In the year preceding major ENSO events, the model captures pronounced amplifications in interaction strength relative to neutral states (1980 or 1991): preceding the strong 1983 El Niño, the TNA influence was 5.04 times higher than in 1991 (Fig. 5l) and 3.14 times higher than in 1980 (Fig. 5k); similarly, the NPMM influence before the 1997 El Niño (Fig. 5j) showed 3.79-fold and 2.64-fold increases relative to 1991 and 1980, respectively. These findings, which emerged without previous physical assumptions, are consistent with independent physics-based simulations identifying the NPMM as a more sustained

https://doi.org/10.1038/s42256-026-01245-5

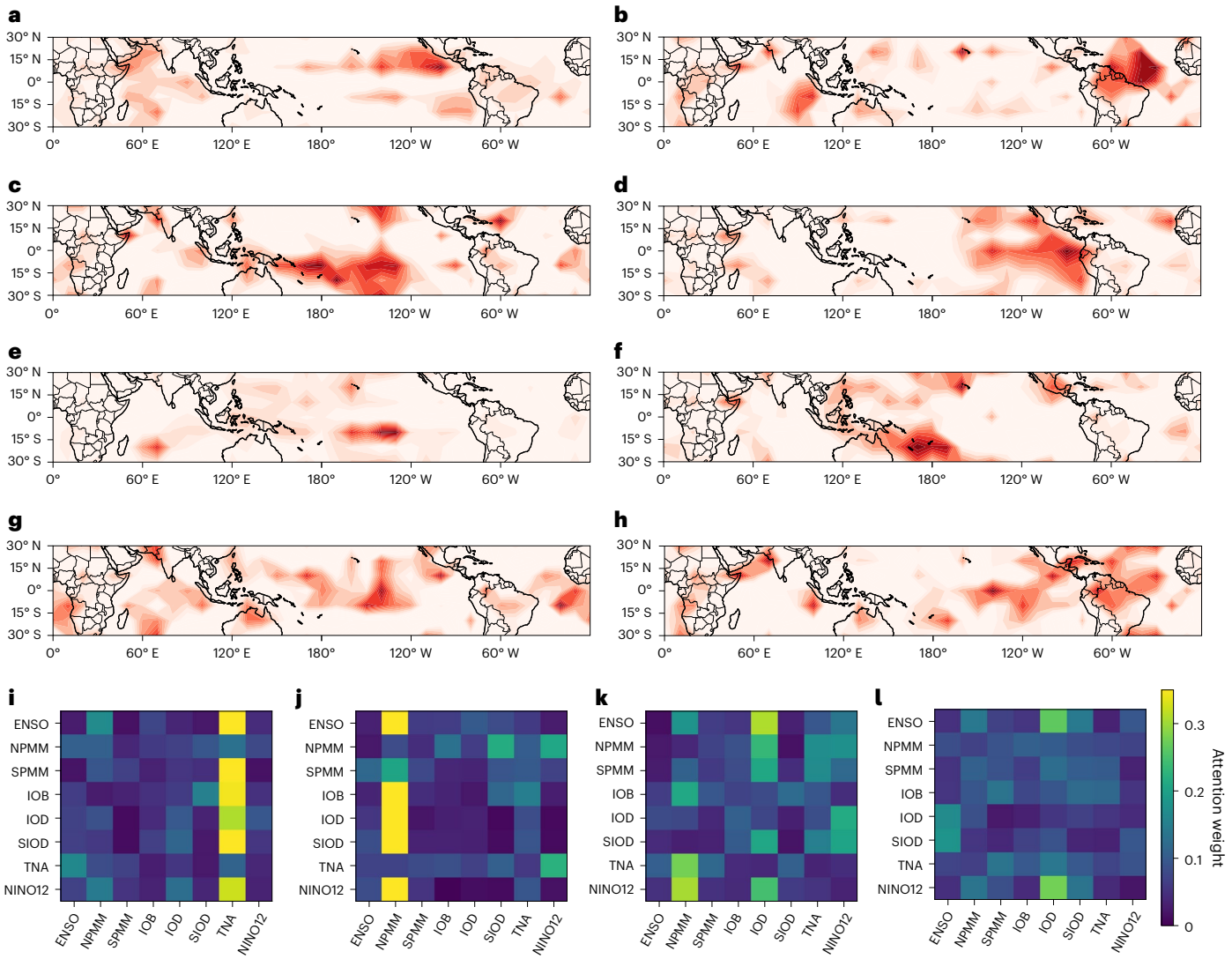

Fig. 5 | UniCM's attention mechanism reveals event-specific precursors to major ENSO events. a–**h**, Spatial attention maps extracted from UniCM for six representative ENSO years (1983 (**a**); 1995 (**b**); 1996 (**c**); 1997 (**d**); 1999 (**e**) and 2010 (**f**)) and two normal years (1980 (**g**) and 1991 (**h**)), which were selected as representative neutral periods with weak climate-mode activity. The colour shading indicates the normalized attention weight, with warmer colours representing geographic regions that the model identified as more critical for prediction. The model focuses on distinct geographical regions, such as the eastern Equatorial Pacific for the 1983 and 1997 El Niños and the tropical Atlantic for the 1995 La Niña, while attention is diffuse during normal years. **i**–**l**, Heatmaps showing the learned interaction strengths (attention weights) between climate modes in the 12 months preceding the same events. Strong, structured interactions, particularly from the NPMM and TNA, emerge before major El Niños (pre-1983 (**i**) and pre-1997 (**j**)), contrasting with the weak, uniform interactions preceding normal years (pre-1980 (**k**) and pre-1991 (**l**)).

driver of ENSO onset than the MJO[29]. Conversely, in the lead-up to normal years, the interaction matrix remains largely uniform, indicating a weakly coupled state. This capability extends to non-canonical extremes often intractable for linear models. For the 1986 NPMM event (Supplementary Fig. 36a), UniCM's attention mechanism identified a sharp surge in inter-mode interaction weights. During the 1994 IOD–TNA–NPMM co-occurrence (Supplementary Fig. 36b), the model uncovered the TNA as an active driver of Indian Ocean variability, suggesting inter-basin teleconnections under-reported in traditional ENSO-centric literature[11,15]. Furthermore, in the complex multi-mode extreme of 2011 (Supplementary Fig. 36c), UniCM autonomously identified the TNA as a dominant 'hub' node coordinating anomalies across both the Pacific and Indian basins. Collectively, these results extend previous climate network studies[48,49] by advancing from grid-based correlation structures to a mode-level dependency framework, providing new insights into early-warning signals and the coupled dynamics of global climate modes.

Discussion

This work demonstrates that a substantial portion of the global climate's predictability is an emergent property of the interactions among climate modes, commonly referred to as teleconnections[15,46]. We show that this predictability can be unlocked by treating these modes not as isolated phenomena but as a single, interconnected system. Our results reveal that the future state of the global system is more predictable than the sum of its parts because the cross-basin couplings are not random noise but fundamental features of Earth's dynamics[15], containing predictive information often discarded by single-mode forecasts[34,35,50] forecasts. By learning these coupled dynamics directly from data, our framework, UniCM, achieves strong predictive skill, extending the forecast horizon for ENSO to 19 months and IOD to 7 months, while substantially improving accuracy for other less-studied modes across the global oceans[13,34].

The physical basis for this success was confirmed by the model's ability to produce high-fidelity forecasts of the underlying SST fields

and to accurately reconstruct observed teleconnections between ocean basins. In this sense, UniCM goes beyond recent ENSO-centric physics-guided approaches, such as XRO[13] and DESN[25]. While DESN improves long-range ENSO prediction by incorporating physically informed climate-mode predictors, it still operates primarily at the level of mode indices. By contrast, UniCM is built on the premise that the predictability of complex climate variability is unlikely to be fully captured by mode indices alone, but also depends on field-level variations in the underlying physical fields, which both give rise to climate modes and mediate their feedback onto the broader system. This cross-scale design is important because it enables the model to learn not only inter-mode couplings, but also the mode-field interactions through which large-scale modes emerge, persist and influence the broader climate system. Consistent with this view, UniCM's gains are reflected not only in stronger long-range ENSO and multi-mode forecast skill, but also in physically realistic SST forecasts and more faithful reconstruction of lagged teleconnections, indicating that physical field evolution carries predictive information beyond mode-index dynamics alone. Notably, we found that fine-tuning the pretrained model on observational reanalysis data did not yield a substantial performance leap (Supplementary Fig. 41). This suggests that UniCM's dual-branch architecture successfully extracts universal physical manifolds, demonstrating a robust 'sim-to-real' generalization capability. Therefore, UniCM's predictive performance is not a statistical artefact of a powerful architecture but reflects a physically meaningful representation of the coupled climate system, making an important step towards using AI to advance process understanding in the geosciences[33].

From a broader perspective, this capability for long-lead, system-level forecasting has profound practical implications, particularly for anticipating compound climate events[51]. The most severe climate impacts, from concurrent continental-scale droughts and floods to widespread marine heatwaves, are often driven by the constructive interference of multiple climate modes[51,52]. Crucially, the likelihood of such compound events is expected to increase in a warming climate, making skilful long-lead forecasts not only beneficial but essential for societal adaptation[51–53]. By modelling the co-evolution of these climate modes, UniCM enables the anticipation of their co-occurrence, allowing early warnings for high-impact events that are missed by single-mode forecasts[51,53]. This offers a critical advantage for climate-sensitive sectors, supporting proactive, multi-month planning for agriculture, disaster response and the management of interconnected water, food and energy systems[1,5].

Beyond its predictive power, UniCM also serves as a tool for scientific discovery. Its interpretable attention mechanisms enable a data-driven interrogation of the climate system, identifying precursors and dynamic relationships without previous physical assumptions. For instance, the model independently uncovered the role of tropical Atlantic SST anomalies as a precursor to the 1995 Pacific La Niña (Fig. 5b) and quantified the elevated influence of the NPMM and TNA in the lead-up to the major 1983 and 1997 El Niño events (Fig. 5i,j). This capability transforms the model from a 'black box' predictor to an interpretable scientific tool that can guide further research. Instead of being confined to testing isolated, predefined hypotheses, such as whether a warm pool in the Atlantic can trigger an El Niño in the Pacific, researchers can use the model's findings to ask more targeted, data-informed questions, such as 'Which inter-basin connections most strongly govern the onset of extreme events?'

While UniCM marks an advance, its improvement is mode-dependent, with smaller gains for modes such as the IOD whose predictability is intrinsically constrained by tight seasonal phase-locking and short decorrelation timescales[54,55]. Future research should focus on three directions. First, integrating processes across timescales, from intra-seasonal phenomena such as the Madden–Julian Oscillation[56] to decadal components such as the Atlantic Meridional Overturning Circulation[57,58], is essential to capture the cross-timescale interactions governing the background climate. Second, combining attention-based insights with symbolic regression[59,60] can help uncover and formalize the explicit governing equations of these complex dynamics[61,62]. Finally, applying UniCM to forecast climate variability under anthropogenic change[9] will reveal how inter-mode relationships shift under global warming[15]. These avenues will translate data-driven discoveries into a deeper theoretical understanding of Earth's interconnected climate system. Beyond geosciences, UniCM offers a general framework for hierarchical, non-stationary systems by jointly modelling localized dynamics and global couplings. Potential applications include whole-brain functional connectomics in neuroscience[30], socio-economic systems[31,63] and trophic interaction networks in ecology[32,64]. More broadly, representing emergent structures in latent space may help uncover complex co-evolutionary dynamics across diverse high-dimensional systems.

Methods

Data

The UniCM framework was trained on historical climate simulations from a curated subset of the Coupled Model Intercomparison Project Phase 6 (CMIP6). Rather than treating all available CMIP6 models as equally valid, we performed a selection process based on each model's ability to reproduce the observed temporal variances of major climate modes on a validation set. We retained four simulations from two model families: CESM2 and EC-Earth3. We caution that applying the framework to unscreened CMIP6 models may degrade performance due to inter-model biases in tropical climate-mode representations.

To ensure the robustness of our model's performance, its predictive skill was comprehensively evaluated against multiple reanalysis datasets, including GODAS, ERA5, ORAS5 and SODA v.2.2.4. We note that ORAS5 and ERA5 share the same prescribed SST boundary conditions (from OSTIA and HadISST2.1.0)[65,66], and therefore do not constitute independent validations for SST-derived climate-mode indices. The independent cross-validation was provided by GODAS and SODA v.2.2.4, which use separately assimilated ocean analyses. All results reported in both the main text and Supplementary Information, including prediction skill metrics, correlation reproduction, spatial patterns and attention-based interpretability analysis, are derived exclusively from these reanalysis datasets, which are used solely for model evaluation. In the main text, ORAS5 is adopted as the primary testing dataset, while results based on other reanalysis products (including GODAS, ERA5 and SODA v.2.2.4) are provided in the Supplementary Sections 2 and 3 for completeness. Supplementary Table 3 provides a detailed summary of all datasets used, including their temporal periods and spatial resolutions, as well as the specific breakdown of the training, validation and testing sets.

We used 165 years of CMIP6 historical runs to provide a climatologically diverse training set. To generate samples, we applied a sliding-window approach with a 1-month stride, where each sample consists of a 12-month input sequence and a 24-month target forecast horizon, resulting in a total of 1,945 samples. Sensitivity analysis (Supplementary Section 5.3) demonstrates that the model's performance depends more on the temporal span (climatological diversity) than on the raw sample count. We found that covering complete multi-decadal physical cycles is essential for generalization, whereas high-frequency sampling (1-month stride) introduces redundancy, suggesting high data efficiency in learning global climate dynamics.

Model overview

The core challenge in forecasting global climate modes lies in modelling the complex, multi-scale feedback loop between fine-grained physical fields and the large-scale climate patterns that emerge from them. From a bottom-up perspective, modes such as ENSO are emergent structures

arising from the dynamics of variables such as SST. From a top-down perspective, these modes become organizing forces that interact and collectively steer the evolution of the broader climate system.

To capture this dual perspective, UniCM is designed as a unified, multi-view Transformer framework. Its architecture consists of two parallel, interacting branches. The Globalformer models the bottom-up process by learning the high-dimensional spatiotemporal dynamics of the underlying physical climate fields. Concurrently, the Modeformer models the top-down influence by explicitly capturing the temporal co-evolution and nonlinear interactions among multiple climate modes (M) across different ocean basins. These two branches are dynamically linked by a cross-view coupling mechanism, which injects the learned high-level mode dynamics into the fine-grained physical field modelling. This design enables UniCM to learn system-wide teleconnections and leverage their emergent predictability, providing a more holistic and powerful forecasting foundation.

Input data and preprocessing

The UniCM framework is trained on two distinct but complementary streams of input data derived from historical climate simulations and reanalysis datasets.

Physical climate fields. To capture the state of the ocean–atmosphere system, we use five key physical variables: SST, zonal surface wind stress (τ_x), meridional surface wind stress (τ_y), thermocline depth (h_T) and the average temperature of the upper 300 m of the ocean (T_{300}). Each variable, represented by the tensor $X^{(c)}$, is preprocessed by first calculating monthly anomalies and then standardizing them using the climatological mean (μ) and standard deviation (σ) for each calendar month:

$$X_t^{(c)} = \frac{X_t^{(c)} - \mu^{(c)}_{\text{month}(t)}}{\sigma^{(c)}_{\text{month}(t)}}, \; c \in \{1, \ldots, 5\}. \tag{1}$$

The resulting fields are interpolated onto a regular 5° × 5° grid covering the global oceans from 40° S to 40° N. This grid is then divided into non-overlapping spatial patches of size $p \times p$. This process converts the input tensor of shape (T_h, H, W, 5) into a sequence of tokens of shape (T_h, N_p, 5), where T_h is the number of historical time steps and $N_p = H/p \times W/p$ is the number of patches. Finally, each patch is linearly projected into the model's hidden dimension $\mathbb{R}^D$ to serve as input for the Globalformer.

Climate-mode indices. In parallel, we process the time series for seven key climate modes: ENSO, IOD, TNA variability, NPMM, SPMM, IOB mode and the SIOD. Each mode index, T_m, is computed from the SST fields according to its standard scientific definition (detailed in Supplementary Table 4) and smoothed with a 3-month running mean to filter out high-frequency noise. The resulting multivariate time series of shape (T_h, M), where $M = 7$, serves as the input for the Modeformer. The model is trained to predict these indices for a future horizon of $T_p = 24$ months.

Unified multi-view Transformer architecture

UniCM's core is a spatiotemporal Transformer that uses an encoder–decoder structure to facilitate autoregressive long-horizon forecasting. A key feature of its design is the decoupling of spatial and temporal attention within each layer, which reduces computational complexity from $\mathcal{O}((TN)^2)$ to $\mathcal{O}(T^2 + N^2)$ and makes it scalable for high-resolution climate data.

Globalformer branch. The Globalformer is designed to learn the evolution of the physical climate fields. Its encoder receives the sequence of patched field data of shape (T_h, N_p, D). Within each layer, it first applies temporal attention independently to each spatial patch's time series, followed by spatial attention across all patches at each time step. This process can be formally expressed as:

$$Z^{(t)}_{t,n} = \text{MSA}_{\text{time}}(Z_{1:T_h,n}), \tag{2}$$

$$Z^{(s)}_{t,n} = \text{MSA}_{\text{space}}\left(\text{Z}^{(t)}_{\text{t,1:N}_p}\right), \tag{3}$$

where $Z_{t,n}$ represents the hidden state of patch n at time t, and $\text{MSA}_{\text{space}}$ captures inter-regional spatial dependencies across the globe. The decoder then autoregressively generates predictions for future physical fields, $\hat{X}_t \in \mathbb{R}^{H \times W \times C}$.

Modeformer branch. The Modeformer operates on the sequence of climate-mode indices of shape (T_h, M, D). Its architecture is analogous to the Globalformer, but its spatial attention mechanism operates across the different climate modes rather than geographical patches. Each Transformer layer alternates temporal and mode-wise self-attention:

$$H^{(t)}_{t,m} = \text{MSA}_{\text{time}}(H_{1:T_h,m}), \tag{4}$$

$$H^{(s)}_{t,m} = \text{MSA}_{\text{mode}}\left(\text{H}^{(t)}_{\text{t,1:M}}\right), \tag{5}$$

where MSA_{time} models the temporal evolution of each mode individually, and MSA_{mode} captures the dynamic interdependencies and couplings between modes. The Modeformer encoder produces a rich representation of these interactions, which the decoder uses to autoregressively forecast future mode indices, $\hat{T}_{m,M}$. Critically, the encoder's output also serves as the high-level guidance signal for the Globalformer.

Encoder–decoder architecture. Both Modeformer and Globalformer adopt encoder–decoder structures to support autoregressive long-horizon forecasting. The Modeformer encoder processes the historical mode-index sequence $I_{1:T_h} \in \mathbb{R}^{T_h \times M}$ using stacked spatiotemporal Transformer layers, producing hidden representations $H_{1:T_h} \in \mathbb{R}^{T_h \times M \times D}$. The Modeformer decoder then autoregressively generates future mode indices $\hat{I}_{T_h:T_h+T_p} \in \mathbb{R}^{T_p \times M}$ by attending to previously predicted values and applying cross-attention to the encoder output. In parallel, the Globalformer encoder encodes the historical physical fields $X_{1:T_h} \in \mathbb{R}^{T_h \times H \times W \times C}$. After spatial patching and projection, these inputs are transformed into a sequence of latent tokens with shape $\mathbb{R}^{T_h \times N_p \times D}$ and processed through a stack of temporal–spatial Transformer layers. The Globalformer decoder then predicts future physical fields $\hat{X}_{T_h:T_h+T_p} \in \mathbb{R}^{H \times W \times C}$ in an autoregressive fashion, conditioned not only on past field predictions but also on the mode-level dynamics captured by the Modeformer, via the cross-view interaction mechanism. This encoder–decoder setup enables UniCM to generate coherent multi-step forecasts by leveraging both fine-grained physical representations and structured climate-mode dependencies.

Cross-view coupling using mode-to-patch guidance. To realize the top-down influence of climate modes on the physical fields, we introduce a cross-view coupling mechanism that injects representations from the Modeformer into the Globalformer at both encoder and decoder stages. This is achieved by adding a mode-conditioned bias to the token embeddings of spatial patches that fall within the geographical region $\mathcal{R}_m$ of a given climate mode m. Let $z_{t,n}$ be the token for patch n and $h_t^{(m)}$ be the learned representation of mode m from the Modeformer. The guidance is implemented as follows:

Encoder-stage guidance:

$$z^{\text{enc}}_{t,n} \leftarrow z^{\text{enc}}_{t,n} + \sum_{m:n \subset R_m} W^{\text{enc}}_m \times h_t^{(m)}, \tag{6}$$

Decoder-stage guidance:

$$z_{t,n}^{\mathrm{dec}} \leftarrow z_{t,n}^{\mathrm{dec}} + \sum_{m:n\subset R_m} W_m^{\mathrm{dec}} \times h_t^{(m)}, \tag{7}$$

where $W_m^{\mathrm{enc}}, W_m^{\mathrm{dec}} \in \mathbb{R}^{D\times D}$ are learned projection matrices specific to each mode m. This mechanism acts as a form of 'mode guidance', forcing the Globalformer's predictions to be consistent with the state of the large-scale climate patterns.

Alternatively, this guidance can be implemented via masked cross-attention:

$$\mathrm{Attn}\,(Q,K,V) = \mathrm{softmax}\left(\frac{QK^{\top}}{\sqrt{d}} + M\right) \times V, \tag{8}$$

where $M_{i,j} = 0$ if patch i belongs to mode region j, and $-\infty$ otherwise. This cross-view mechanism ensures that local physical predictions are dynamically informed by global climate drivers.

In summary, UniCM integrates global-mode dynamics with local physical fields through this dual-branch synergy. Notably, while the Modeformer branch generates direct mode-index predictions ($\hat{I}_{\mathrm{M}}$), these are designated as auxiliary outputs to provide high-level dynamic guidance rather than the final evaluation results. Our final forecasts are based on the indices derived from the Globalformer's predicted physical fields ($\hat{I}_{\mathrm{G}}$). This design choice is grounded in the observation that the Globalformer, once enhanced by the Modeformer's guidance, can leverage richer spatiotemporal information from the full physical fields to achieve superior predictive accuracy. Empirical evaluations also justify this design. First, the Globalformer-derived indices outperform direct Modeformer outputs (Supplementary Fig. 37b). Furthermore, ablation studies on integration strategies (Supplementary Fig. 37a) show that our 'additive guidance' outperforms a 'replacement' strategy, indicating that the Modeformer's representations effectively complement rather than substitute the fundamental dynamics captured by the Globalformer.

Training objective

The UniCM framework is trained end-to-end using a composite objective function $\mathcal{L}$ that balances three complementary goals, ensuring that the model learns a physically consistent and coherent representation of the climate system. The function is as follows:

$$\mathcal{L} = \lambda_1 \underbrace{\text{m.s.e.}(\hat{X}, X)}_{\mathcal{L}_{\mathrm{field}}} + \lambda_2 \underbrace{\sum_{m\in M} \text{m.s.e.}(\hat{I}_{\mathrm{G}}, I)}_{\mathcal{L}_{\mathrm{global-mode}}} + \lambda_3 \underbrace{\sum_{m\in M} \mathrm{MSE}(\hat{I}_{\mathrm{M}}, I)}_{\mathcal{L}_{\mathrm{mode-aux}}} \tag{9}$$

The three components are defined as follows. First, the physical field reconstruction loss ($\mathcal{L}_{\mathrm{field}}$) is the primary objective for the Globalformer. It minimizes the m.s.e. between the predicted physical fields $\hat{X}$ and the ground-truth fields X across the entire forecast horizon, ensuring the model generates high-fidelity, spatially resolved forecasts. Second, the global-mode consistency loss ($\mathcal{L}_{\mathrm{global-mode}}$) enforces consistency between the two views. This term supervises the climate-mode indices $\hat{I}_{\mathrm{G}}$ that are derived from the Globalformer's predicted SST field against the ground-truth indices I. It encourages the Globalformer to preserve the correct large-scale spatial patterns that define each climate mode. Finally, the Modeformer auxiliary loss ($\mathcal{L}_{\mathrm{mode-aux}}$) is a crucial auxiliary objective that directly supervises the mode indices $\hat{I}_{\mathrm{M}}$ predicted by the Modeformer.

The final loss is a weighted sum of these three components, with hyperparameters λ_1, λ_2 and λ_3 balancing their contributions. In our experiments, these were set to $\lambda_1 = 1$, $\lambda_2 = 1$ and $\lambda_3 = 0.01$ to ensure all objectives were meaningfully optimized. This multi-objective formulation guides UniCM to learn a robust, multi-scale representation of the global climate system.

Implementation details

Model architecture. Both Modeformer and Globalformer use hidden dimension $D = 256$. The Modeformer consists of 8 Transformer layers (4 encoder layers and 4 decoder layers), each with 4 attention heads and a feedforward network of intermediate dimension 512. The Globalformer adopts the same configuration and includes eight stacked layers. Spatial attention in Globalformer is applied over $N_{\mathrm{p}} = 12 \times 72$ spatial patches, corresponding to a 5° × 5° resolution over the global ocean grid. Mode-to-patch guidance is implemented via learnable linear projection heads of shape 256 for each climate mode. A complete list of hyperparameters is detailed in Supplementary Table 2.

Experimental setup. To ensure the reproducibility of our results, we define the forecasting task as follows. The targets of UniCM are the monthly mean anomalies of the climate indices. The lead time is defined as the number of months from the end of the input sequence to the target month. For example, if the input sequence ends in December, a 1-month lead forecast targets January of the following year. We use a sliding-window protocol for model initialization: the input window (length L) slides forward by 1 month at each step to generate a continuous sequence of forecasts across the entire evaluation period.

All models are trained using the AdamW optimizer with an initial learning rate of 5×10^{-4} and a weight decay of 1×10^{-6}. We use a linear warm-up over the first three epochs, followed by a cosine decay schedule. We use a batch size of 32. Gradient clipping is applied with a global ℓ_2 norm threshold of 1.0. Dropout with a rate of 0.2 is used in both the attention and feedforward sublayers. The model is trained for 200 epochs, and the best checkpoint is selected based on the validation loss evaluated over the target prediction horizon. To ensure determinism and evaluate the model's sensitivity to initialization, we conduct all experiments across 20 independent runs with fixed random seeds (1–20). All reported performance metrics (for example, ACC, r.m.s.e.) represent the mean values across these 20 runs to ensure statistical significance. All experiments are conducted using a single NVIDIA A100 GPU (80 GB) with PyTorch v.2.0. The typical training time for 1 model is ~6 GPU-hours. A full summary of the hyperparameters is provided in Supplementary Table 2.

Model selection and validation. Our validation–test split is performed temporally within the reanalysis data: we use the period before 1980 for validation and the period after 1980 for testing. Model selection is based on the mean forecast skill aggregated across multiple climate modes, evaluated using the corresponding climate-mode indices (derived from SST). As UniCM is designed primarily for climate-mode forecasting, auxiliary physical fields (for example, surface wind stress, thermocline depth and upper-ocean temperature) are treated as input coupling fields and are not used as separate validation targets in our current setup.

Data availability

All datasets used in this study are publicly available. The CMIP6 data are available from https://cds.climate.copernicus.eu/datasets/projections-cmip6; the ORAS5 data are available from the Climate Data Store (CDS) at https://cds.climate.copernicus.eu/datasets/reanalysis-oras5; the ERA5 data are available from CDS at https://cds.climate.copernicus.eu/datasets/reanalysis-era5-single-levels-monthly-means; the GODAS data are available from the National Oceanic Atmospheric Administration Physical Science Laboratory at https://psl.noaa.gov/data/gridded/data.godas.html; and the SODA data are available from the SODA project at https://soda.umd.edu/.

Code availability

The source code for UniCM is publicly available via GitHub at https://github.com/tsinghua-fib-lab/UniCM-Global-Climate-Modes and via Zenodo at https://doi.org/10.5281/zenodo.19173780 (ref. 67).

References

1. Lobell, D. B., Schlenker, W. & Costa-Roberts, J. Climate trends and global crop production since 1980. *Science* **333**, 616–620 (2011).
2. Dettinger, M. D. & Diaz, H. F. Global characteristics of stream flow seasonality and variability. *J. Hydrometeorol.* **1**, 289–310 (2000).
3. Bracco, A. et al. Machine learning for the physics of climate. *Nat. Rev. Phys.* **7**, 6–20 (2025).
4. Philander, S. G. H. El Nino Southern Oscillation phenomena. *Nature* **302**, 295–301 (1983).
5. IPCC *Climate Change 2021: The Physical Science Basis* (eds Masson-Delmotte, V. et al.) (Cambridge Univ. Press, 2021).
6. Deser, C., Alexander, M. A., Xie, S.-P. & Phillips, A. S. Sea surface temperature variability: patterns and mechanisms. *Annu. Rev. Mar. Sci.* **2**, 115–143 (2010).
7. McPhaden, M. J., Zebiak, S. E. & Glantz, M. H. ENSO as an integrating concept in earth science. *Science* **314**, 1740–1745 (2006).
8. Timmermann, A. et al. El Niño–Southern Oscillation complexity. *Nature* **559**, 535–545 (2018).
9. Cai, W. et al. Changing El Niño–Southern Oscillation in a warming climate. *Nat. Rev. Earth Environ.* **2**, 628–644 (2021).
10. Zhou, L. & Zhang, R.-H. A self-attention–based neural network for three-dimensional multivariate modeling and its skillful ENSO predictions. *Sci. Adv.* **9**, eadf2827 (2023).
11. Saji, N., Goswami, B. N., Vinayachandran, P. & Yamagata, T. A dipole mode in the tropical Indian Ocean. *Nature* **401**, 360–363 (1999).
12. Webster, P. J., Moore, A. M., Loschnigg, J. P. & Leben, R. R. Coupled ocean–atmosphere dynamics in the Indian Ocean during 1997–98. *Nature* **401**, 356–360 (1999).
13. Zhao, S. et al. Explainable El Niño predictability from climate mode interactions. *Nature* **630**, 891–898 (2024).
14. Shaw, T. A. & Stevens, B. The other climate crisis. *Nature* **639**, 877–887 (2025).
15. Cai, W. et al. Pantropical climate interactions. *Science* **363**, eaav4236 (2019).
16. Jin, Y. et al. The Indian Ocean weakens the ENSO spring predictability barrier: role of the Indian Ocean basin and dipole modes. *J. Clim.* **36**, 8331–8345 (2023).
17. Jo, H.-S. et al. Southern Indian Ocean dipole as a trigger for Central Pacific El Niño since the 2000s. *Nat. Commun.* **13**, 6965 (2022).
18. Alexander, M. A., Shin, S.-I. & Battisti, D. S. The influence of the trend, basin interactions, and ocean dynamics on tropical ocean prediction. *Geophys. Res. Lett.* **49**, e2021GL096120 (2022).
19. Cai, W., Van Rensch, P., Cowan, T. & Hendon, H. H. Teleconnection pathways of ENSO and the IOD and the mechanisms for impacts on Australian rainfall. *J. Clim.* **24**, 3910–3923 (2011).
20. Dijkstra, H. A. *Nonlinear Climate Dynamics* (Cambridge Univ. Press, 2013).
21. Chiang, J. C. & Vimont, D. J. Analogous Pacific and Atlantic meridional modes of tropical atmosphere–ocean variability. *J. Clim.* **17**, 4143–4158 (2004).
22. Vos, E., Huybers, P. & Tziperman, E. Climate change alters teleconnections. *Geophys. Res. Lett.* **53**, e2025GL119307 (2026).
23. Ling, F. et al. Multi-task machine learning improves multi-seasonal prediction of the Indian Ocean dipole. *Nat. Commun.* **13**, 7681 (2022).
24. Luo, J.-J. et al. Interaction between El Nino and extreme Indian Ocean dipole. *J. Clim.* **23**, 726–742 (2010).
25. Zhang, Z. et al. Enhancing the predictability limits of ENSO with physics-guided deep echo state networks. *NPJ Clim. Atmos. Sci.* **9**, 92 (2026).
26. Wang, B. et al. Understanding the recent increase in multiyear La Niñas. *Nat. Clim. Change* **13**, 1075–1081 (2023).
27. Heede, U. K. & Fedorov, A. V. Colder eastern Equatorial Pacific and stronger Walker circulation in the early 21st century: separating the forced response to global warming from natural variability. *Geophys. Res. Lett.* **50**, e2022GL101020 (2023).
28. Jiang, S., Zhu, C., Hu, Z.-Z., Jiang, N. & Zheng, F. Triple-dip La Niña in 2020–23: understanding the role of the annual cycle in tropical Pacific SST. *Environ. Res. Lett.* **18**, 084002 (2023).
29. Liang, Y., Xie, S.-P., Fedorov, A. & Yeager, S. G. North pacific meridional mode has larger impacts on El Niño evolution than the March Madden–Julian oscillation. *Sci. Adv.* **11**, eadv8621 (2025).
30. Bassett, D. S. & Sporns, O. Network neuroscience. *Nat. Neurosci.* **20**, 353–364 (2017).
31. Helbing, D. Globally networked risks and how to respond. *Nature* **497**, 51–59 (2013).
32. Allesina, S. & Tang, S. Stability criteria for complex ecosystems. *Nature* **483**, 205–208 (2012).
33. Reichstein, M. et al. Deep learning and process understanding for data-driven earth system science. *Nature* **566**, 195–204 (2019).
34. Ham, Y.-G., Kim, J.-H. & Luo, J.-J. Deep learning for multi-year ENSO forecasts. *Nature* **573**, 568–572 (2019).
35. Lyu, P. et al. Resonet: robust and explainable ENSO forecasts with hybrid convolution and transformer networks. *Adv. Atmos. Sci.* **41**, 1289–1298 (2024).
36. Duan, W., Liu, X., Zhu, K. & Mu, M. Exploring the initial errors that cause a significant 'spring predictability barrier' for El Niño events. *J. Geophys. Res. Oceans* **114**, C04022 (2009).
37. Jin, F.-F. An equatorial ocean recharge paradigm for ENSO. Part I: conceptual model. *J. Atmos. Sci.* **54**, 811–829 (1997).
38. Ashok, K., Behera, S. K., Rao, S. A., Weng, H. & Yamagata, T. El Niño Modoki and its possible teleconnection. *J. Geophys. Res. Oceans* **112**, (2007).
39. Kao, H.-Y. & Yu, J.-Y. Contrasting Eastern-Pacific and Central-Pacific types of ENSO. *J. Clim.* **22**, 615–632 (2009).
40. Simpson, I. R. et al. Confronting Earth system model trends with observations. *Sci. Adv.* **11**, eadt8035 (2025).
41. Ham, Y.-G., Kug, J.-S., Park, J.-Y. & Jin, F.-F. Sea surface temperature in the north tropical Atlantic as a trigger for El Niño/Southern Oscillation events. *Nat. Geosci.* **6**, 112–116 (2013).
42. Guo, F., Liu, Q., Yang, J. & Fan, L. Three types of Indian Ocean basin modes. *Clim. Dyn.* **51**, 4357–4370 (2018).
43. Zhang, H., Clement, A. & Di Nezio, P. The South Pacific meridional mode: a mechanism for ENSO-like variability. *J. Clim.* **27**, 769–783 (2014).
44. Chen, L. et al. A machine learning model that outperforms conventional global subseasonal forecast models. *Nat. Commun.* **15**, 6425 (2024).
45. Wang, L. et al. Cas-Canglong: a skillful 3D transformer model for sub-seasonal to seasonal global sea surface temperature prediction. Preprint at https://doi.org/10.48550/arXiv.2409.05369 (2024).
46. Alexander, M. A. et al. The atmospheric bridge: the influence of ENSO teleconnections on air–sea interaction over the global oceans. *J. Clim.* **15**, 2205–2231 (2002).
47. Schwing, F. B., Murphree, T., deWitt, L. & Green, P. M. The evolution of oceanic and atmospheric anomalies in the Northeast Pacific during the El Niño and La Niña events of 1995–2001. *Prog. Oceanogr.* **54**, 459–491 (2002).
48. Fan, J., Meng, J., Ashkenazy, Y., Havlin, S. & Schellnhuber, H. J. Network analysis reveals strongly localized impacts of El Niño. *Proc. Natl Acad. Sci. USA* **114**, 7543–7548 (2017).
49. Meng, J. et al. Complexity-based approach for El Niño magnitude forecasting before the spring predictability barrier. *Proc. Natl Acad. Sci. USA* **117**, 177–183 (2020).
50. Chen, Y. et al. Combined dynamical-deep learning ENSO forecasts. *Nat. Commun.* **16**, 3845 (2025).

51. Zscheischler, J. et al. Future climate risk from compound events. *Nat. Clim. Change* **8**, 469–477 (2018).
52. AghaKouchak, A. et al. Climate extremes and compound hazards in a warming world. *Annu. Rev. Earth Planet. Sci.* **48**, 519–548 (2020).
53. Raymond, C. et al. Understanding and managing connected extreme events. *Nat. Clim. Change* **10**, 611–621 (2020).
54. McKenna, S., Santoso, A., Gupta, A. S., Taschetto, A. S. & Cai, W. Indian Ocean dipole in CMIP5 and CMIP6: characteristics, biases, and links to ENSO. *Sci. Rep.* **10**, 11500 (2020).
55. Yang, Y. et al. Seasonality and predictability of the Indian Ocean dipole mode: ENSO forcing and internal variability. *J. Clim.* **28**, 8021–8036 (2015).
56. Zhang, C. Madden–Julian oscillation. *Rev. Geophys.* **43**, (2005).
57. Rahmstorf, S. Ocean circulation and climate during the past 120,000 years. *Nature* **419**, 207–214 (2002).
58. Buckley, M. W. & Marshall, J. Observations, inferences, and mechanisms of the Atlantic meridional overturning circulation: a review. *Rev. Geophys.* **54**, 5–63 (2016).
59. Schmidt, M. & Lipson, H. Distilling free-form natural laws from experimental data. *Science* **324**, 81–85 (2009).
60. Udrescu, S.-M. & Tegmark, M. AI Feynman: a physics-inspired method for symbolic regression. *Sci. Adv.* **6**, eaay2631 (2020).
61. Camps-Valls, G. et al. Discovering causal relations and equations from data. *Phys. Rep.* **1044**, 1–68 (2023).
62. Zanna, L. & Bolton, T. Data-driven equation discovery of ocean mesoscale closures. *Geophys. Res. Lett.* **47**, e2020GL088376 (2020).
63. Chinazzi, M. et al. The effect of travel restrictions on the spread of the 2019 novel coronavirus (COVID-19) outbreak. *Science* **368**, 395–400 (2020).
64. Rohr, R. P., Saavedra, S. & Bascompte, J. On the structural stability of mutualistic systems. *Science* **345**, 1253497 (2014).
65. Hirahara, S., Balmaseda, M. A., Boisseson, E. & Hersbach, H. *Sea Surface Temperature and Sea Ice Concentration for ERA5* Vol. 26 (European Centre for Medium Range Weather Forecasts, 2016).
66. Zuo, H., Balmaseda, M. A., Tietsche, S., Mogensen, K. & Mayer, M. The ECMWF operational ensemble reanalysis–analysis system for ocean and sea ice: a description of the system and assessment. *Ocean Sci.* **15**, 779–808 (2019).
67. Yuan, Y., Ding, J., Qiu, Z., Fan, J. & Li, Y. Code for learning the coupled dynamics of global climate modes. *Zenodo* https://doi.org/10.5281/zenodo.19173780 (2026).

Acknowledgements

This work was supported in part by the National Key Research and Development Program of China (grant no. 2024YFC3307603), the National Natural Science Foundation of China (grant no. 62476152) and the Tsinghua–Toyota Joint Research Institute Interdisciplinary Program to Y.L. and J.D. J.F. received support from the National Natural Science Foundation of China (grant nos. T2525011, 42450183, 12275020, 12135003 and 42461144209) and the National Key R&D Program of China (grant no. 2025YFF0517203). J.F. acknowledges support from the Fundamental Research Funds for the Central Universities.

Author contributions

Y.L. and J.F. conceived of the main theme of the research idea. Y.Y. collected the data, designed the model, conducted the experiments and wrote the first draft of the paper. J.D., Z.Q., J.F. and Y.L. provided crucial feedback. All authors reviewed, edited and approved the final version of the paper.

Competing interests

The authors declare no competing interests.

Additional information

Supplementary information The online version contains supplementary material available at https://doi.org/10.1038/s42256-026-01245-5.

Correspondence and requests for materials should be addressed to Jingfang Fan or Yong Li.

Peer review information *Nature Machine Intelligence* thanks Annalisa Bracco, Maximilian Gelbrecht and Jing-Jia Luo for their contribution to the peer review of this work. Peer reviewer reports are available.